CALCULATION OF THE ENERGY DEPOSITION OF ELECTRON CYCLOTRON WAVES IN A STELLARATOR PLASMA

Z.X. ZHANG

IPP 2/264 November 1982

MAX-PLANCK-INSTITUT FÜR PLASMAPHYSIK

8046 GARCHING BEI MÜNCHEN

MAX-PLANCK-INSTITUT FÜR PLASMAPHYSIK

GARCHING BEI MÜNCHEN

CALCULATION OF THE ENERGY DEPOSITION OF ELECTRON CYCLOTRON WAVES IN A STELLARATOR PLASMA

Z.X. ZHANG

IPP 2/264 November 1982

Permanent Address: Institute of Physics,
Academia Sinica. Now working in IPP,
8046 Garching, FRG as an Alexander
Humboldt stipendiat

Die nachstehende Arbeit wurde im Rahmen des Vertrages zwischen dem Max-Planck-Institut für Plasmaphysik und der Europäischen Atomgemeinschaft über die Zusammenarbeit auf dem Gebiete der Plasmaphysik durchgeführt.

Abstract

Based on a three-dimensional ray-tracing code, the energy deposition profiles of the electron cyclotron O-mode and X-mode at the first harmonic calculated. The finite antenna aperture is taken into account. The energy deposition profiles are given in one dimensional form, which is related to the magnetic surfaces and can be used in transport code. The effects of the antenna aperture, the oblique angle of the axis of the antenna to the meridian plane or to the equatorial plane and the plasma parameters to the energy deposition are studied.

Introduction

This paper is a continuation of a previous work [4]. In the previous work the electron cyclotron emission (ECE) line profiles of the X-mode at the second harmonic for different W-VII A plasma parameters were calculated. The reliability of measuring temperature profiles by ECE was checked. Now the code is modified into a modular structure. The present work is aimed at ECRH purposes. We calculate the energy deposition profiles and the single pass energy deposition of the O-mode at first harmonic (injected from the low-field side) and that of the X-mode at first harmonic (injected from the high field side). The wave frequency is 28 GHz. Ray-tracing is carried out in three dimensions, but the energy deposition on magnetic surfaces is calculated by finding out the cross-points of the considered ray with the magnetic surfaces. So the energy deposition profiles are given in one-dimensional form, which is convenient for transport calculations. The antenna is modeled as a cone, consisted of 25 rays, everyone of which may have a different weight function. The final energy depostion is an average over these 25 rays.

Calculation Procedure

The three-dimensional ray-tracing is carried out by using the Appleton-Hartree equation as dispersion equation [3]. Since W-VII A is a machine with large aspect ratio (major radius 2 meters, effective minor radius 10 cm), the helical field at every point is calculated by using a straight helical approximation.
The used temperature distribution function is

$$T_e(\rho,\Theta,\varphi,) \; / \; T_o = 1 \; / \left(1 + \left(\frac{XH(\rho,\Theta,\varphi)}{X_t}\right)^{A_1}\right) \qquad (1)$$

where the effective radius XH is a function of the quasi-cylindrical coordinates ρ,Θ,φ.

Its contours in poloidal plane are ellipses which rotate along the toroidal direction. X_t is a constant quantity, T_o is the temperature at the plasma centre, A_1 is a constant. The used density distribution function is

$$n_e(\rho,\theta,\varphi) \;/\; n_o = 1 \;/\left(1 + \left(\frac{XH(\rho,\theta,\varphi)}{X_d}\right)^{A_2}\right) \qquad (2)$$

where $XH(\varphi,\theta,\varphi)$ is the same function as in formula (1), X_d is a constant quantity, A_2 is a constant, n_o is the density at the plasma centre.

The antenna is modeled as a cone, consisting of 25 rays, which are shown in Fig. 1. Three different antenna patterns are used, which are shown in Fig. 2. The pattern C is an one-ray model (only the central ray is considered).

The relative energy absorption is an average over these 25 rays:

$$RSA = 1 - \sum_{i=1}^{25} W_i I(i) \qquad (3)$$

where W_i is the weight function of the i-th ray, determined by the geometry of the antenna, and

$$I(i) = \exp\left(-\int_o^s \alpha(s')ds'\right) \qquad (4)$$

where integration is carried out along the considered ray. $\alpha(s')$ is the absorption coefficient at point s'. We use formulas given in reference [1]for the absorption coefficient in the finite density region. The perpendicular propagation or the oblique propagation is distinguished according to the primary direction of the wave vector.

The calculation of an energy deposition profile is carried out in following way. We divide the x-axis into many equal intervals

by points a,..., d, e, f,... (see Fig. 3), the first point a is at the plasma centre. For every point, saying point d, there is a density contour passing through it. We find out the cross points A and A' of the considered ray with this contour and calculate the power deposited at the neighbourhood of point A and point A'. This power is assumed to be distributed into the whole toroidal magnetic flux tube which includes contour d and has the selected depth (0.001 metre). If r is the distance of point d from the centre, the deposited power per unite volume is expressed as

$$P_i(r) = \frac{1}{2}\Big(\alpha(A)n_r^2(A)\exp\Big(-\int_o^{S_A}\alpha(s)ds\Big) + \alpha(A')n_r^2(A')\times$$

$$\exp\Big(-\int_o^{S_{A'}}\alpha(s)ds\Big)\Big)/\big(0.001\times 2\pi R_o \ell(r)\big) \qquad (5)$$

where n_r should be the ray refractive index, but we simply use the refractive index n, $\ell(r)$ is the circuit of the contour d. The averaged energy deposition profile is given by

$$P(r) = P_o\sum_{i=1}^{25} W_i P_i(r)\ ,\ P_o \text{ is the input power} \qquad (6)$$

In the code we calculate the relative ratios of the deposited energy on different contours according to formula (5) and normalize the deposition distribution to the value of the single pass energy deposition.

Calculated Results

In all the calculations, the wave frequency is 28 GHz, the injected wave power is 100 KW. The parameters for T_e profile and for n_e profile are: X_T = 0.06(meter), X_D = 0.05(meter), A_1=10, A_2 = 5.00. Antenna pattern A is used in most of the cases, except particularly indicated. The value of the rotational transform is ι = 0.23, except in some special cases.

In all the ray-tracing figures, there are cross-marks on the rays, which show the position where $\frac{eB}{m_o} = \omega$ (ω is the wave frequency, m_o is the rest mass of electron, B is the local magnetic field).

1. O-mode, first harmonic, injected from the low-field side.

Let us first see the effects of different angles between the axis of the antenna and the equatorial plane. Some results are shown in Fig. 4 to Fig. 7, where the oblique angle of the axis of the antenna to the meridian plane is zero. We can see that, both the single pass energy deposition and the energy deposition profile are strongly effected by this angle. This fact can be understood by examing the ray-tracing figures: the absorption region is moved when the angle is changed. Besides, from Fig. 8 we can see that the energy is deposited into a very narrow region. The quite large single pass energy deposition at a temperature of 400eV is due to the large major radius of W-VII A (2 metres).

The effect of changing the density n_o at the plasma centre on the energy deposition is shown in Fig. 8 to Fig. 11. We can see that, if the central density n_o is less than about 70% of the cut-off density, the single pass energy deposition is approximately proportional to the density; when n_o is close to the cut-off density, the absorption is strongly dropped. This is due to the refractive effect. Furthermore, the energy deposition profile will move outward, when the density rises. Viewing these figures, one should remember that the energy deposition profile is given as a function of absorbed power per unit volume versus radius. The bigger the radius is, the larger is the corresponding volume.

In the case of perpendicular propagation of the O-mode, both the single pass energy deposition and the energy deposition profile

are strongly influenced by the value of the magnetic field. This situation is shown in Fig. 12. A change of the magnetic field for about 2% may cause very obvious change in energy deposition. The current in the helical winding may also effect the energy deposition. When the transform ι from a value of 0.35 rises to 0.630, the peak of the energy deposition profile moves about 1cm out-ward and the single pass energy deposition has a change of 4% for the case of B_o = 1.0T, $n_o = 5 \times 10^{12}/cm^3$ and T_o = 400eV.

The effects of plasma temperature to absorption are shown in Fig. 13 and Fig. 14. When the temperature drops, the absorption drops and the profile becomes narrower.

The effects of different antenna patterns are shown in Fig. 15. We see that neither the single pass energy deposition nor the energy deposition profile is strongly effected by the antenna patterns. For the considered three antenna patterns, the deviation of the single pass energy deposition is not more than 6% from each other.

2. X-mode, first harmonic, injected from the high field side.

The absorption of the X-mode at first harmonic is strongly effected by the oblique angle of the wave vector to the magnetic field (or to the meridian plane - poloidal plane). When it propagates perpendicular to the magnetic field, the absorption is very weak, but when the wave vector deviates from the poloidal plane by a angle of 20^o, the absorption is already larger than that of the O-mode at first harmonic under the same plasma parameters. This situation is shown in Figures 16-19. From the ray-tracing figures and from a CMA diagram (Fig. 21) we can also see that the rays stop at the upper-hybrid layer. Another striking character is that the absorption region of the X-mode at the oblique propagation case is much wider than that of the O-mode at first harmonic in perpendicular propagating case. This is

why the single pass absorption of the X-mode at oblique propagating case is not strongly effected by the change of the magnetic field, although the profile obviously is changed (see Fig. 20). Here we would like to point out that, if the resonance line is moved to the outside of the upper-hybrid layer by a change in magnetic field the situation will be strongly different.

Another striking character in case of the X-mode at first harmonic in oblique propagating case is that within the finite density region ($\frac{\omega_p^2}{\omega^2} > 2 \frac{V_t}{C} N \cdot \cos\theta$, see ref.[1]), the absorption increases when the density drops. This is shown in Fig. 22, where the dotted line implies a tenuous plasma region. As for the dependence of the absorption to temperature, the X-mode has almost the same character as that of the O-mode (see Fig. 23).

Some Discussions

A machine like the W VII-A with a large major radius is a good machine for ECRH experiment. If the experimental purpose is to obtain additional heating, then it would be expected to have the highest heating efficiency with the wave in X-mode (obtained by mode conversion from the output of a gyrotron), injected from the high field side of the plasma and propagating oblique to the magnetic field (oblique angle to the poloidal plane more than 20°). The other advantage of using such a mode is that the plasma density under which the heating efficiency is good is higher than by using the O-mode at the first harmonic.

If the experimental purpose is aimed at obtaining temperature profile control, especially for feedback control of the disruptive instability of a Tokamak plasma, the O-mode at first the harmonic, injected from the low-field side and propagating perpendicular to the magnetic

field, is a good candidate, since its energy deposition will be localized in a very narrow region. One may select the heating region by changing the oblique angle of the antenna to the equatorial plane or by changing the toroidal magnetic field a little (only about 2% is needed).

If the experimental purpose is aimed at heating a "cold" plasma (starting-up experiment), a mode conversion processes may be considered, such as the O-mode to X-mode to electron Bernstein mode conversion, proposed by the IPF group [2]. In this aspect, more detailed study is necessary.

Acknowledgement

This work is supported by Alexander von Humboldt - Stiftung and the IPP. Many discussions with Dr. H. Wobig should be acknowledged. Thanks to Dr. G. von Gierke and Dr. G. Grieger for much help.

References

[1] Bornatici M. (1980). Proceedings of the Joint Workshop on Electron Cyclotron Emission and Electron Cyclotron Resonance Heating, Oxford, Culham Report CLM-ECR

[2] Erckmann V., Erz U., Janzen G., Moser F., Müller G., Räuchle E., Schwörer K., Schüller P. G., Thumm M., Wilhelm R. (1982) IPF Report

[3] Ott E., Hui B., Chu K. R. (1980) Phys. Fluids 23, 1031

[4] Zhang Z. X. (1982) IPP 2/263

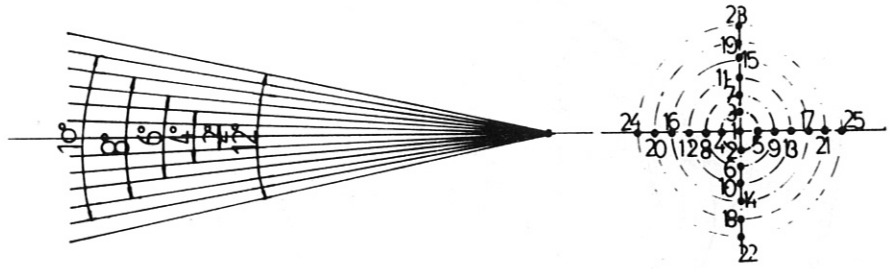

ANTENNA MODEL

Fig. 1 Antenna model

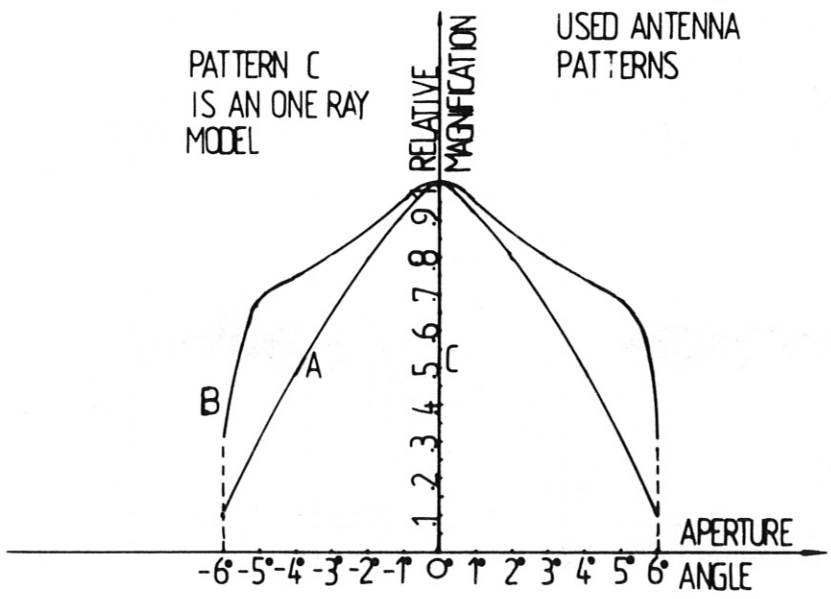

Fig. 2 Used antenna patterns

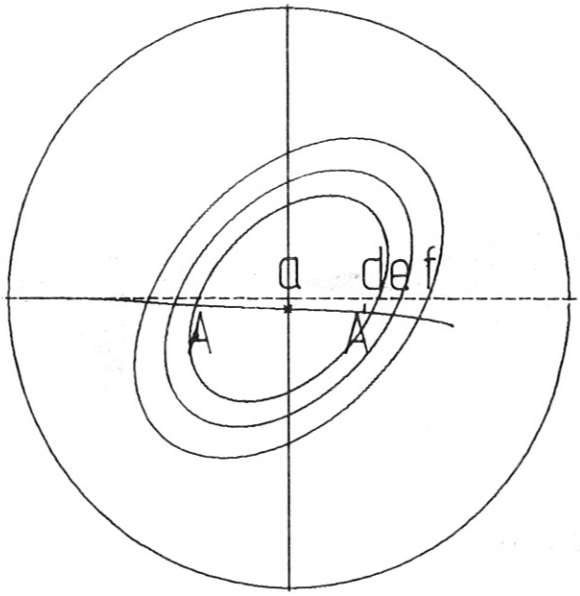

Fig. 3

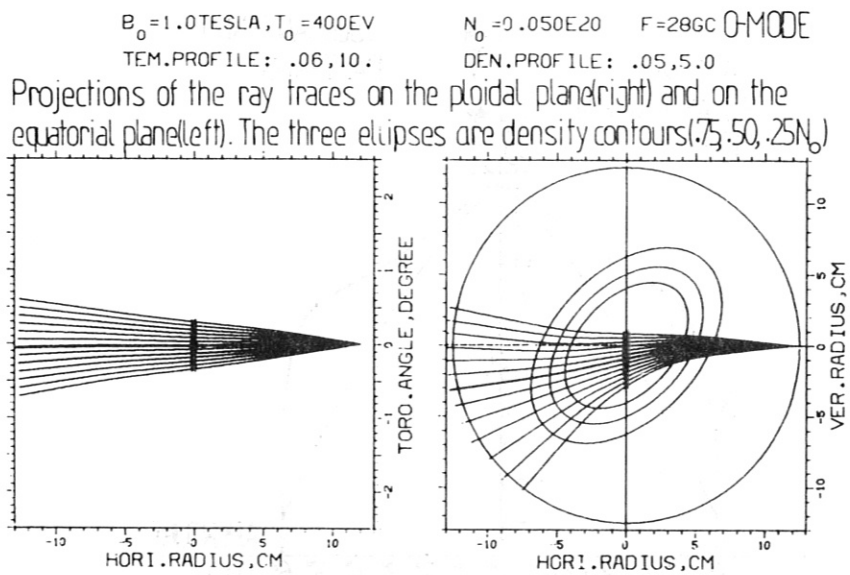

Fig. 4 Traces under PANG $=-5^{\circ}$. PANG is the oblique angle of the axis of the antenna to the equatorial plane.

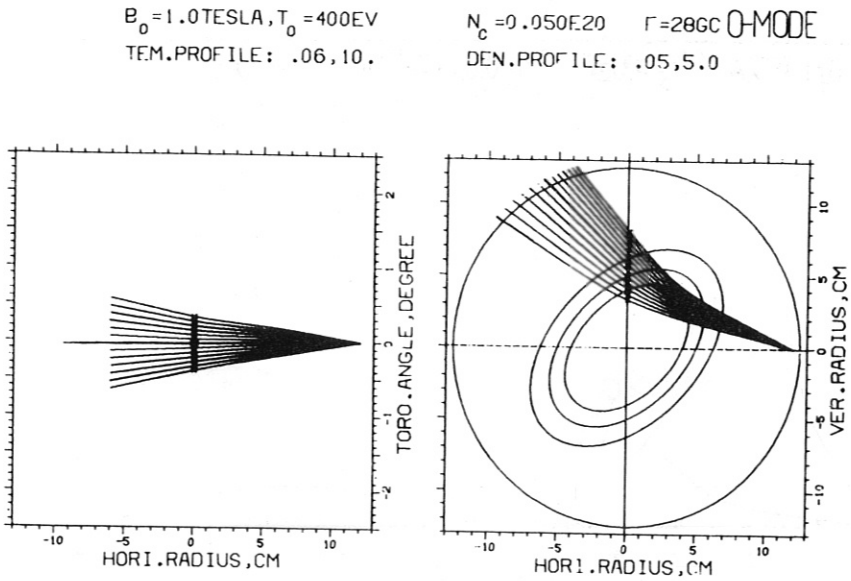

Fig. 5 Traces under $P_{ANG} = 20^{o}$

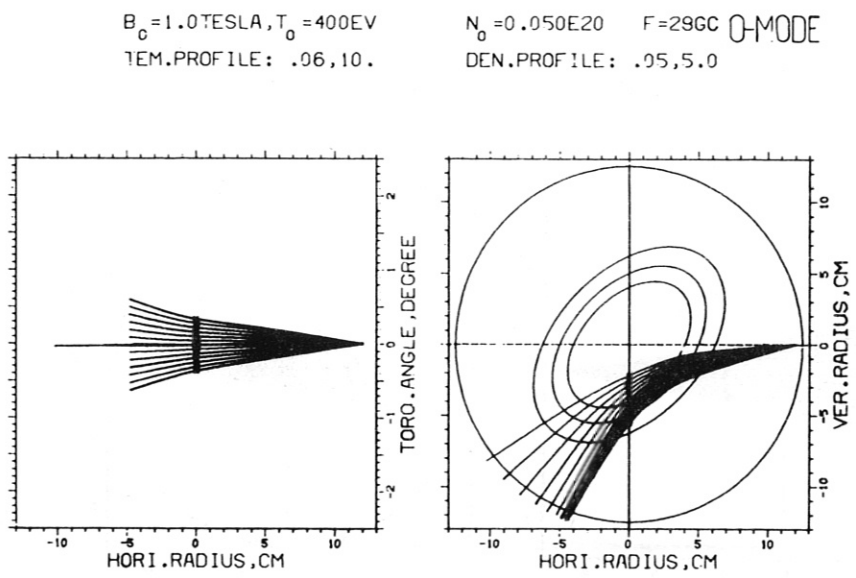

Fig. 6 Traces under $P_{ANG} = -10^{o}$

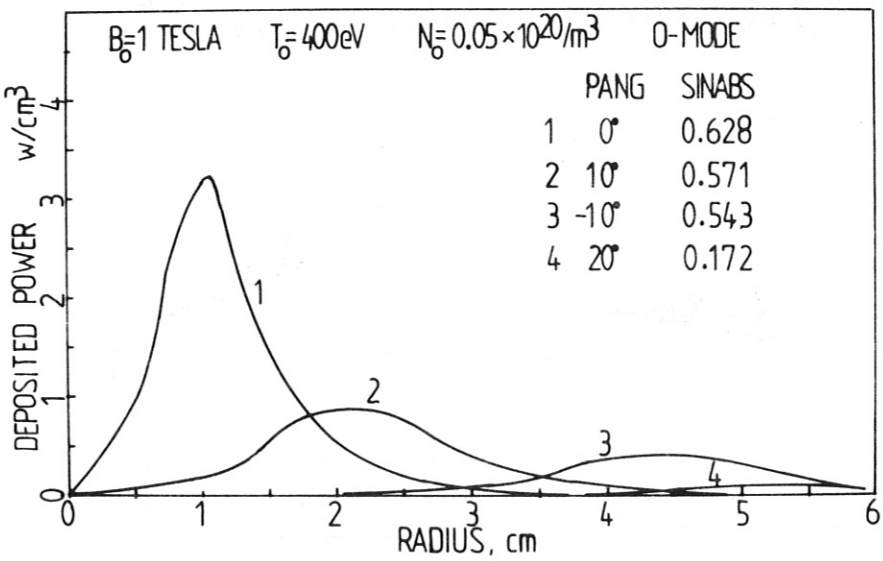

Fig. 7 Energy deposition profiles under different PANG values, where 'SINABS' means single pass energy absorbtion.

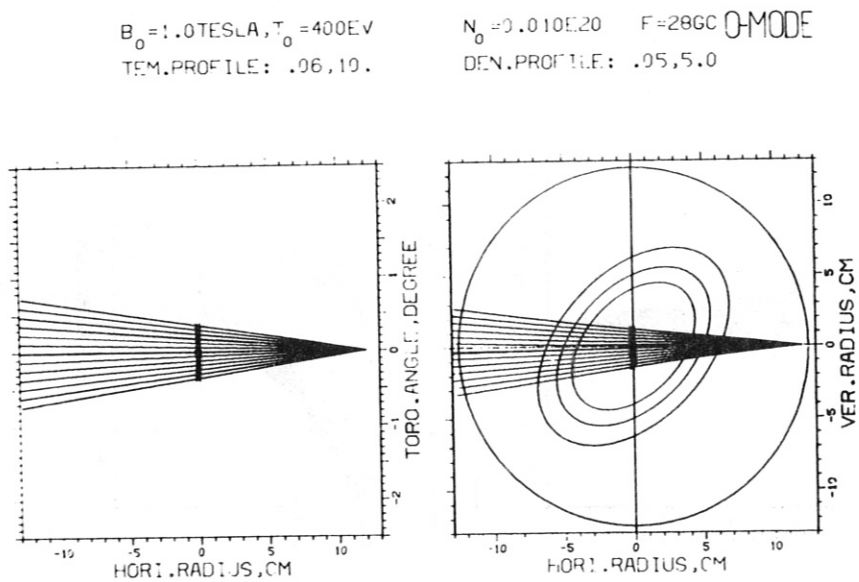

Fig. 8 Traces under $N_o = 0.01 \times 10^{20}/m^3$. N_o is the density at the plasma centre.

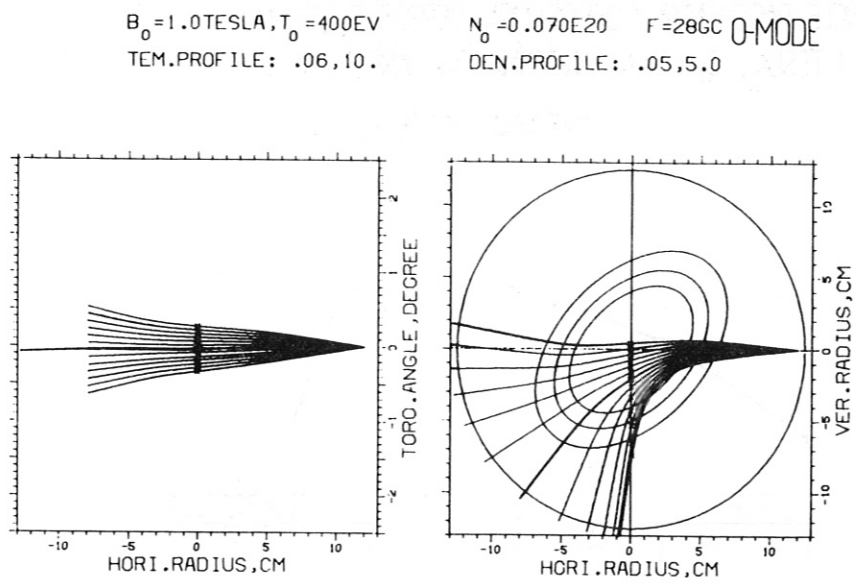

Fig. 9 Traces under $N_o = 0.07 \times 10^{20}/m^3$

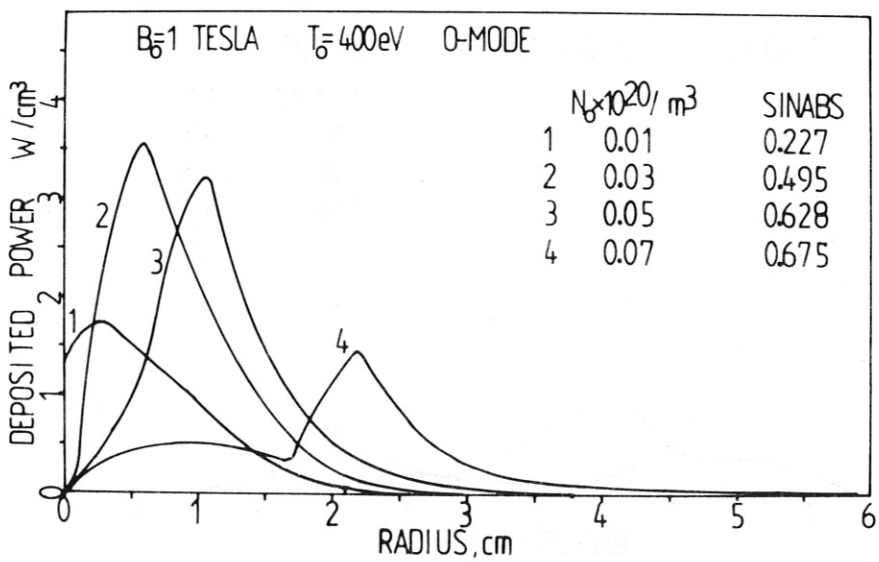

Fig. 10 Energy deposition profiles under different N_o values

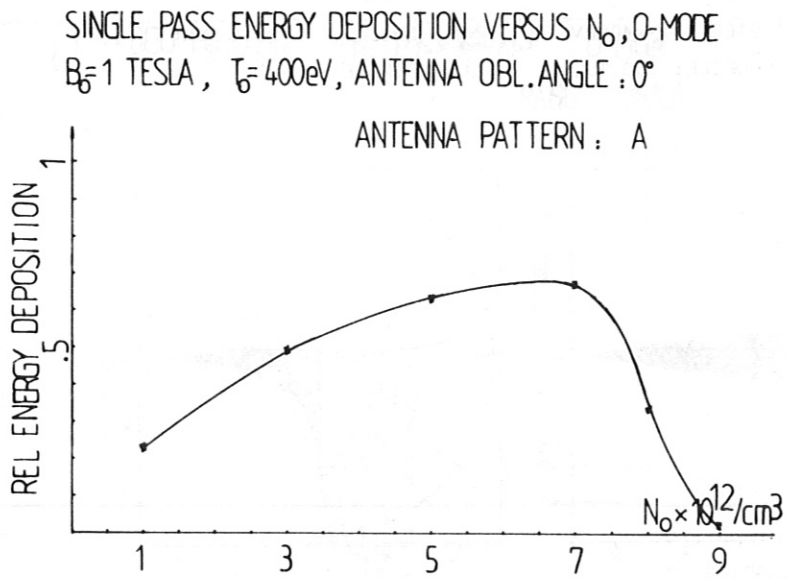

Fig. 11 Single pass energy deposition versus N_o.

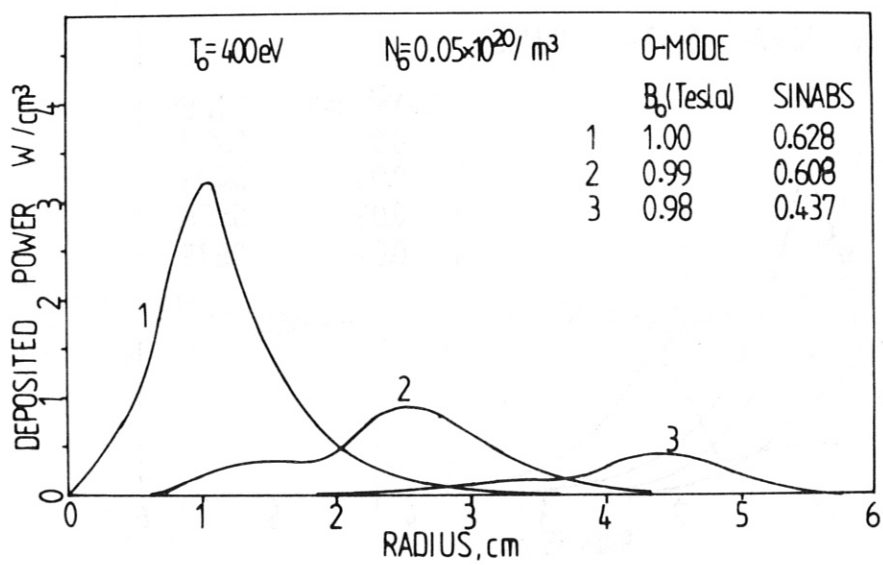

Fig. 12 Energy deposition profiles under different B_o values. B_o is the toroidal field at the plasma centre.

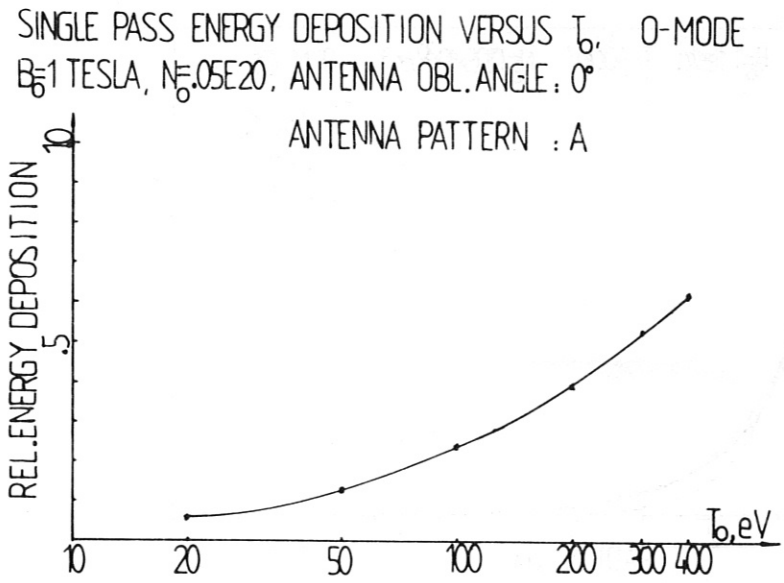

Fig. 13 Single pass energy deposition versus T_o. T_o is the temperature at the plasma centre.

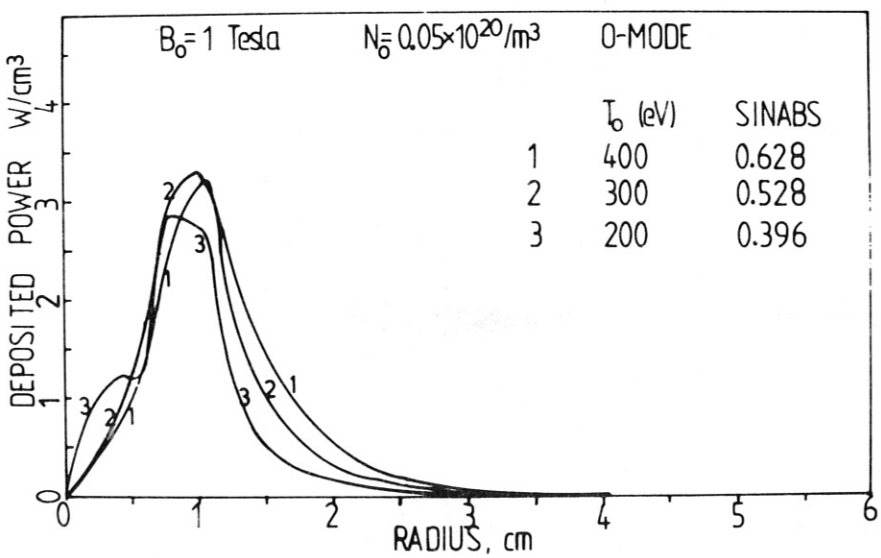

Fig. 14 Energy deposition profiles under different T_o values.

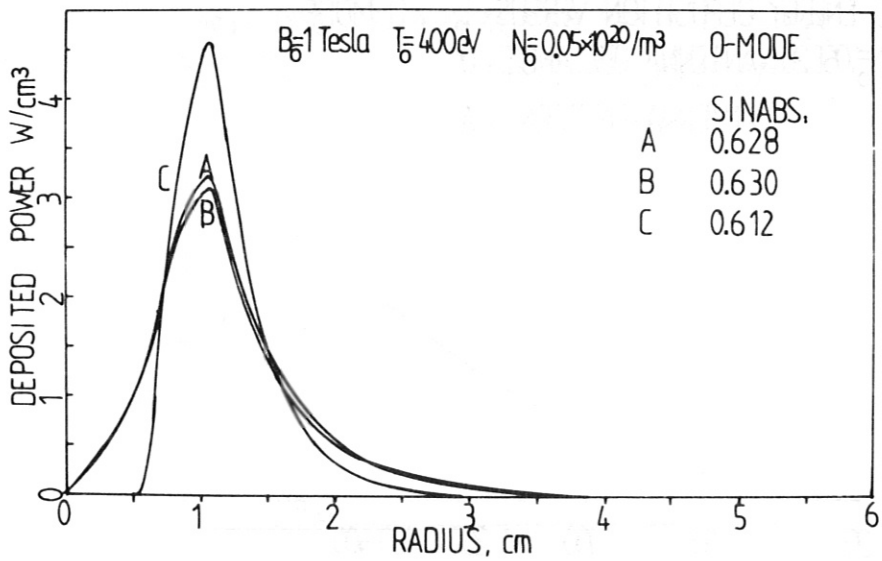

Fig. 15 Energy deposition profiles for different antenna patterns. Patterns A, B and C are defined in Fig. 2.

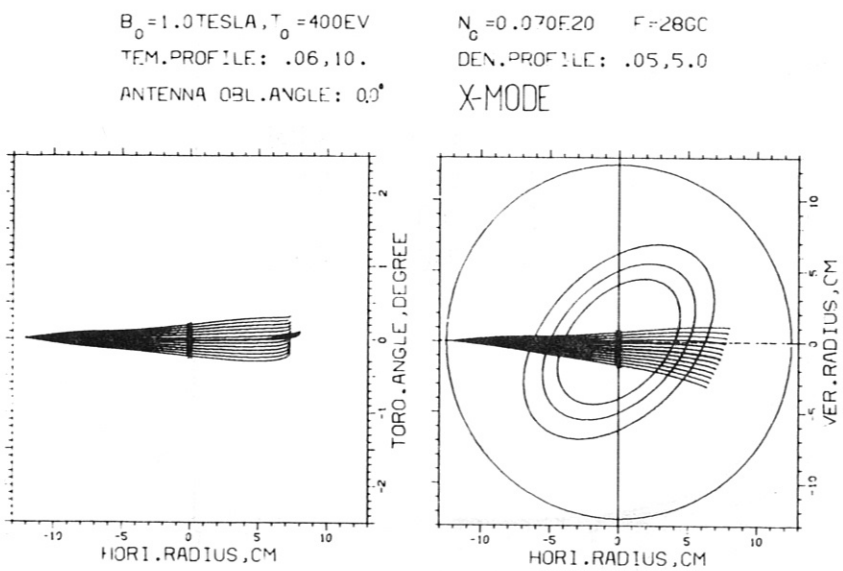

Fig. 16 Traces under FANG = 0^{o}. FANG is the oblique angle of the axis of the antenna to the maridian plane.

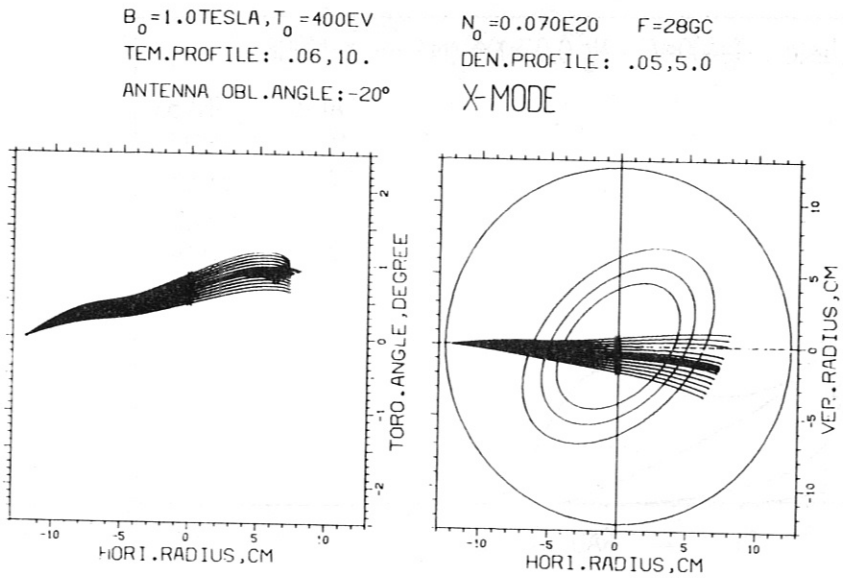

Fig. 17 Traces under FANG = 20°

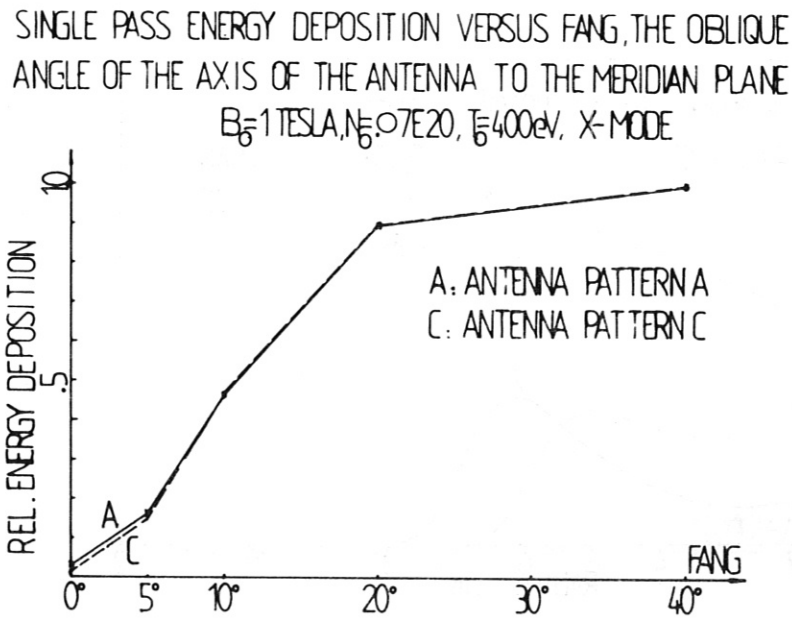

Fig. 18 Single pass energy deposition versus FANG.

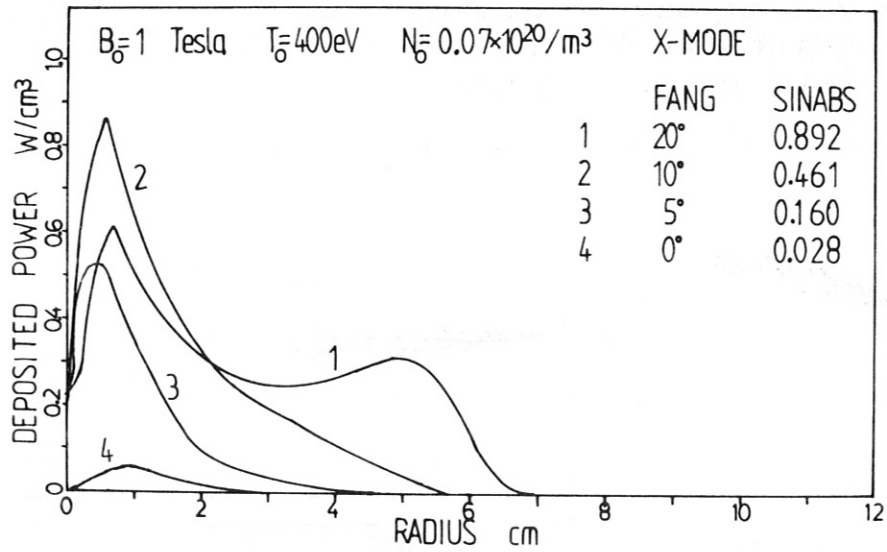

Fig. 19 Energy deposition profiles under different FANG values.

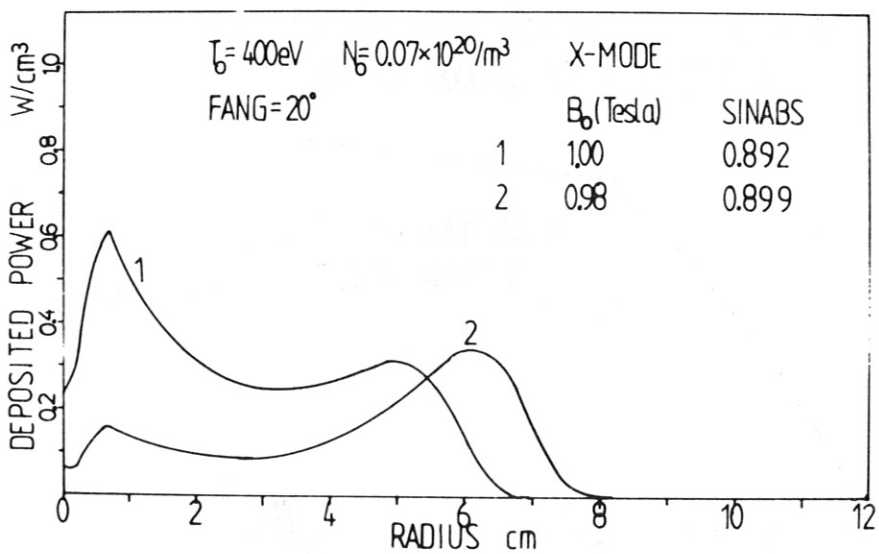

Fig. 20 Energy deposition profiles under different B_o values.

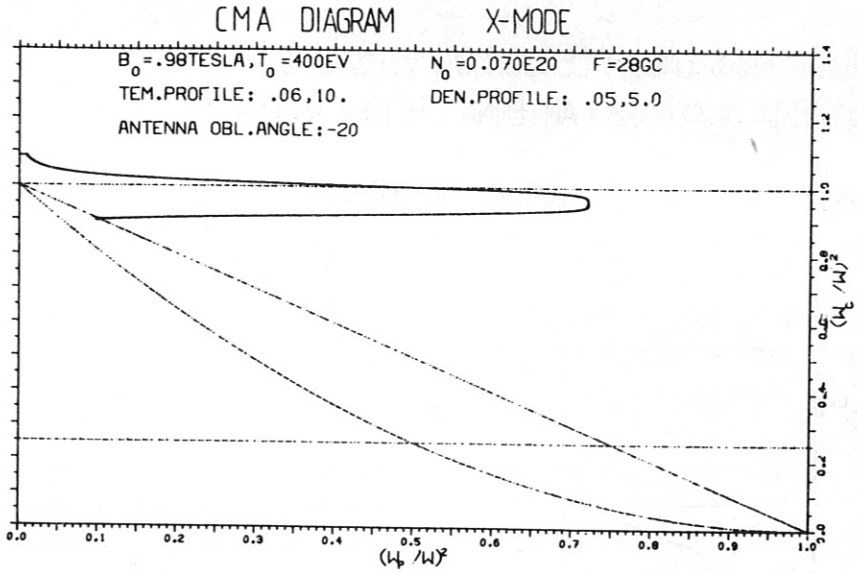

Fig. 21 CMA diagram of the 14-th ray (see Fig. 1)

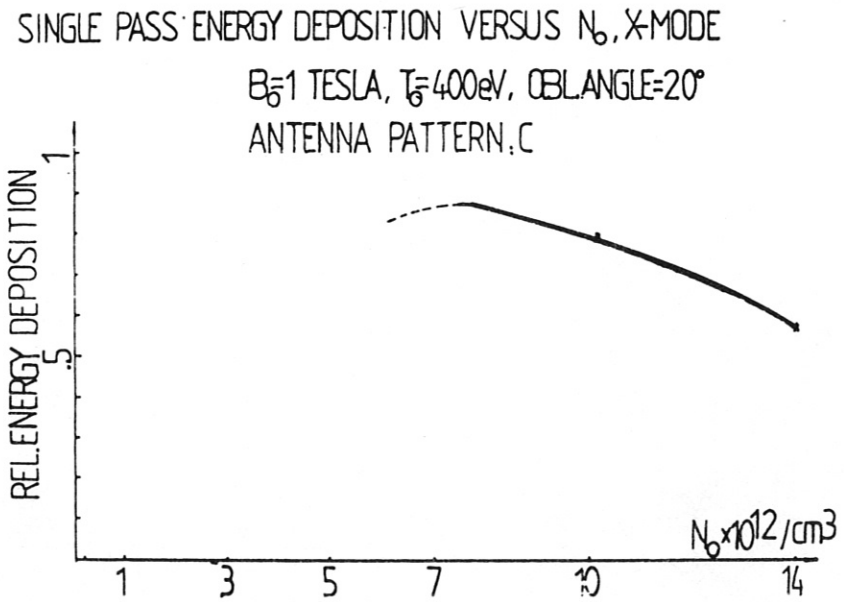

Fig. 22 Single pass energy deposition versus N_o

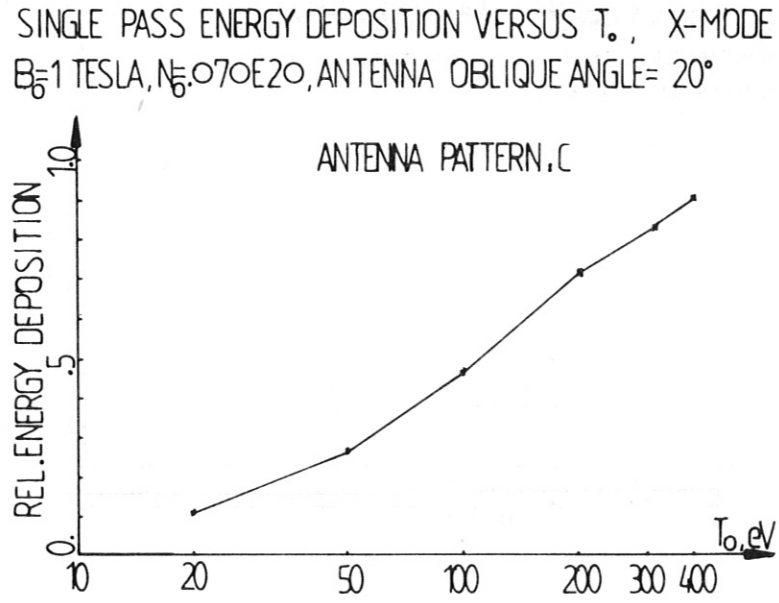

Fig. 23 Single pass energy deposition versus T_o.